ORIGINAL ARTICLE

CrossMark

Two Diverse Hemodynamic Forces, a Mechanical Stretch and a High Wall Shear Stress, Determine Intracranial Aneurysm Formation

Hirokazu Koseki[1,2,3] · Haruka Miyata[1,3,4] · Satoshi Shimo[5] · Nobuhiko Ohno[6,7] · Kazuma Mifune[8] · Kenjiro Shimano[8] · Kimiko Yamamoto[9] · Kazuhiko Nozaki[4] · Hidetoshi Kasuya[2] · Shuh Narumiya[10] · Tomohiro Aoki[1,3,10]

Abstract

Intracranial aneurysm (IA) usually induced at a bifurcation site of intracranial arteries causes a lethal subarachnoid hemorrhage. Currently, IA is considered as a macrophage-mediated inflammatory disease triggered by a high wall shear stress (WSS) on endothelial cells. However, considered the fact that a high WSS can be observed at every bifurcation site, some other factors are required to develop IAs. We therefore aimed to clarify mechanisms underlying the initiation of IAs using a rat model. We found the transient outward bulging and excessive mechanical stretch at a prospective site of IA formation. Fibroblasts at the adventitia of IA walls were activated and produced (C-C motif) ligand 2 (CCL2) as well in endothelial cells loaded on high WSS at the earliest stage. Consistently, the mechanical stretch induced production of CCL2 in primary culture of fibroblasts and promoted migration of macrophages in a Transwell system. Our results suggest that distinct hemodynamic forces, mechanical stretch on fibroblasts and high WSS on endothelial cells, regulate macrophage-mediated IA formation.

Keywords Intracranial aneurysm · Hemodynamic force · Stretch · Fibroblast · Macrophage

Introduction

Intracranial aneurysm (IA) is a regional bulging of an intracranial artery mainly located at its bifurcation site. IA is mostly an asymptomatic lesion as a nature because of its relatively small size, about 5 mm in diameter at average [1]. However, once ruptured, a devastating subarachnoid hemorrhage or rarely other type of hemorrhagic stroke develops. Even today, despite of modern technical advancement in medical care and tremendous effort, treatment of aneurysmal subarachnoid hemorrhage is still quite challenging and indeed, this disease has quite a poor outcome, a high mortality rate up to 50%, and a considerable

✉ Tomohiro Aoki
  tomoaoki@ncvc.go.jp

1 Department of Molecular Pharmacology, Research Institute, National Cerebral and Cardiovascular Center, 5-7-1 Fujishiro-dai, Suita, Osaka 565-8565, Japan

2 Department of Neurosurgery, Tokyo Women's Medical University Medical Center East, Tokyo 116-8567, Japan

3 Core Research for Evolutional Science and Technology (CREST) from Japan Agency for Medical Research and Development (AMED), Kyoto University Graduate School of Medicine, Kyoto 606-8501, Japan

4 Department of Neurosurgery, Shiga University of Medical Science, Shiga 520-2192, Japan

5 Department of Occupational Therapy, Health Science University, Yamanashi 401-0380, Japan

6 Division of Neurobiology and Bioinformatics, National Institute for Physiological Sciences, Aichi 444-8787, Japan

7 Department of Anatomy, Jichi Medical University, Tochigi 329-0498, Japan

8 Department of Mechanical Systems Engineering, Tokyo City University, Tokyo 158-8557, Japan

9 System Physiology, Department of Biomedical Engineering, Graduate School of Medicine, The University of Tokyo, Tokyo 113-0033, Japan

10 Alliance Laboratory for Advanced Medical Research, Medical Innovation Center, Kyoto University Graduate School of Medicine, Kyoto 606-8507, Japan

 Springer

morbidity rate [2]. The prevention of rupture of IAs is thus fundamental for a social health. However, today, a whole picture of the pathogenesis of IAs, how IA initiates, progresses and ruptures, still remains elusive. To treat unruptured IAs properly and prevent a resultant subarachnoid hemorrhage, a whole process from initiation to rupture of IAs and molecular machineries regulating each process should be elucidated.

Recent series of experimental findings mainly from animal models and histopathological studies of human specimen have revealed the crucial contribution of macrophage-mediated inflammatory responses in intracranial arterial walls to IA formation and progression [3–5]. For example, genetic deletion of monocyte chemoattractant protein-1 (MCP-1; (C-C motif) ligand 2 (CCL2)) or administration of the dominant negative form of CCL2 (7-ND) significantly suppresses IA formation and progression in animal models through almost complete inhibition of macrophage recruitment to the lesion [4]. Consistently, pharmacological depletion of macrophages by clodronate liposome again significantly suppresses IA formation [6]. Furthermore, in some experimental conditions in which CCL2 expression is suppressed such as deficiency in a responsible transcription factor for CCL2 expression, NF-κB, IA formation, and progression are greatly suppressed as well [7]. Intriguingly, inhibition of NF-κB activation or deficiency of a prostaglandin E receptor subtype EP2, which mediates NF-κB-regulated inflammation in lesions, specifically in macrophages, suppresses inflammatory responses not only in macrophages but also inflammation in the whole lesion [5]. Macrophage-mediated inflammation in intracranial arterial walls thus leads to IA formation and also progression. Here, as macrophages in IA lesions can form auto-amplification loop via producing their own chemoattractant protein CCL2 [8], infiltration of only a small number of macrophages at the earliest stage may be important event leading to IA formation.

In another point of view, accumulating evidence in 3D-computational fluid dynamic (CFD) analyses of IA lesions have implied a crucial role of hemodynamic force loading on intracranial arteries to IA formation and progression [9–11]. For example, high wall shear stress (WSS) can be detected at prospective sites of IA formation, bifurcation sites of intracranial vasculature [10], and at the neck portion of IA lesions in humans [12]. Also, in animal models, experimental IAs are specifically induced at sites with high WSS and high WSS gradient [9]. From these findings, currently, IA is considered as a hemodynamic stress-sensitive and especially a high WSS-induced disease in intracranial arteries [11]. However, much remains to be elucidated; for example, whether high WSS is a sole important factor triggering the initiation of IAs, what happens at the earliest stage of IA formation under high WSS condition, or how macrophages infiltrate and accumulate in lesions under specific hemodynamic condition.

In the present study, we analyzed the earliest events leading to IA formation mainly using a rat model of IAs and found a previously unknown hemodynamic force-dependent mechanism triggering macrophage accumulation and IA formation.

Methods

Detailed methods are available in Online Resource 1.

Rodent IA Models and Histological Analysis of Induced IA

Male Sprague–Dawley rats were purchased from Japan SLC (Shizuoka, Japan). Transgenic rat expressing GFP specifically in endothelial cells (W-Tg(Tek-GFP)1Soh) were supplied by the National BioResource Project-Rat at Kyoto University (Stock Number #0604, Kyoto, Japan, http://www.anim.med.kyoto-u.ac.jp/NBR/). To induce IA, under general anesthesia by intraperitoneal injection of pentobarbital sodium (50 mg/kg), 7-week-old male rats were subjected to ligation of the left carotid artery and systemic hypertension, induced by the combination of salt overloading and ligation of the left renal artery. Immediately after the surgical procedure, animals were fed the chow containing 8% sodium chloride and 0.12% 3-aminopropionitrile (Tokyo Chemical Industry, Tokyo, Japan), an inhibitor of lysyl oxidase that catalyzes the cross-linking of collagen and elastin, to make extracellular matrix of arterial walls fragile and to facilitate IA formation [5]. At times indicated in the corresponding figure legends or "Results" after aneurysm induction, animals were deeply anesthetized by intraperitoneal injection with a lethal dose of pentobarbital sodium, and transcardially perfused with 4% paraformaldehyde. The right anterior cerebral artery (ACA) and olfactory artery (OA) bifurcation including the induced IA lesion was then stripped, and serial frozen sections were prepared. IA induction at this bifurcation was histopathologically examined after Elastica van Gieson staining. From these images, a size of IAs and a length of disruption of internal elastic lamina were measured using Fiji (https://fiji.sc/). Some specimens were analyzed by a transmission electron microscopy (TEM), scanning electron microscopy (SEM), and serial block-face SEM (SBF-SEM).

Immunohistochemistry

Immunohistochemical analyses were performed as previously described [5]. Briefly, at the indicated period after aneurysm induction, 5-μm-thick frozen sections were prepared. After blocking with 3% donkey serum (Jackson ImmunoResearch, Baltimore, MD), slices were incubated with primary antibodies followed by incubation with secondary antibodies conjugated with a fluorescence dye (Jackson ImmunoResearch).

Finally, fluorescent images were acquired on a confocal fluorescence microscope system (LSM-710, Carl Zeiss Microscopy GmBH, Jena, Germany). The primary antibodies used in this experiment are described in Online Resource 1.

Live-Imaging of Intracranial Arteries of Rats

ACA-OA bifurcation with surrounding intracranial vasculature of W-Tg (Tek-GFP)1Soh rats was surgically exposed under the general anesthesia (pentobarbital sodium, 50 mg/kg) and morphology and motion of arterial walls at this bifurcation site were visualized by expression of fluorescent protein GFP specifically in endothelial cells using a multiphoton-laser confocal microscopy system (A1MP, Nikon Instech Co., Ltd., Tokyo, Japan).

Clodronate Liposome

Clodronate liposome (30 mg/kg, FormuMax Scientific Inc., Sunnyvale, CA) was intraperitoneally administered to rats twice, first at 1 day before and second 2 days after aneurysm induction. At fifth day after aneurysm induction, animals were sacrificed and IA formation including thinning of media, disruption of internal elastic lamina, and cell count of infiltrated macrophage in lesions was assessed as described above. Proper depletion of macrophages by treatment with clodronate liposome was also confirmed in spleen from a treated animal (Online Resource 2).

In Vivo Vascular Permeability Assay

In vivo vascular permeability assay and its analysis were performed as previously described [13, 14]. Rats were subjected to the IA induction as described above. At adequate time after induction, animals were deeply anesthetized and the right common carotid artery was surgically exposed. After clamping the proximal side with a micro serrefine (FST, Foster City, CA), Evans blue (45 mg/kg, Wako Pure Chemical Industries, Ltd., Osaka, Japan) was injected intra-arterially and immediately after the injection rats were transcardially perfused with 4% paraformaldehyde. Frozen sections were then prepared as described above and fluorescent images of Evans blue (excitation wavelength; 620 nm per emission wavelength; 680 nm) [15] were obtained with a confocal fluorescence microscope system (LSM-710, Carl Zeiss Microscopy GmBH). Choroid plexus of a treated animal was also harvested as a positive control specimen because this structure physiologically lacks a blood-brain barrier (Online Resource 3). The acquired images were converted to binary images after adjustment of color threshold, and positively stained area larger than 4-pixel square at ACA-OA bifurcation were included in the analysis using a Fiji.

Primary Culture of Fibroblast from Adventitia in Human Aorta and Stimulation

The primary culture of fibroblasts from adventitia of human aorta (hAoFB) was purchased from Cell Applications (3014-05a, Lot#2366, San Diego, CA). The characteristics of these cells were confirmed by expression of an intermediate filament, vimentin, in immunohistochemistry (mouse monoclonal anti-vimentin antibody, DAKO, Agilent Technologies, Santa Clara, CA) (Online Resource 4a). Cells were maintained in the special medium obtained from the company (Fibroblast Growth Medium 2 Kit, Cell Applications). Cells within P5 were served to experiments.

Cell Stretch Assay

Stretch of cultured cells was achieved by applying these cells to a stretch chamber system from STREX INC. (Osaka, Japan). Briefly, the stretch chamber was coated by 1% gelatin and 0.3 mg/mL of type I-C collagen purified from porcine skin (Nitta Gelatin, Osaka, Japan) overnight and cells were then cultured. The chamber with cultured fibroblasts on its surface was subjected to a uniaxial cyclic stretch (5, 10, 15, and 20% at 1 Hz) for an indicated time period.

Transwell Assay

The chemotaxis of THP-1 cells was assessed using a Transwell system (pore size 5.0 μm, Corning, Corning, NY). THP-1 cells and supernatant of hAoFB culture incubated on the stretch chamber loaded with or without a uniaxial cyclic stretch were added to an upper and a lower chamber, respectively. In some experiment, human recombinant CCL2 (100 ng/mL, R&D Systems) was served as a positive control. After incubation for 3 h, migrating cells in a lower chamber were quantified using a Cell Titer Glo Kit (Promega Corporation, Madison, WI).

Quantitative Real Time-PCR Analysis

RNA purification from cultured cells and reverse transcription were done using an RNeasy Plus Mini Kit (QIAGEN, Hilden, Germany) and a high-capacity cDNA Reverse Transcription Kit (Life Technologies Corporation, Carlsbad, CA) according to manufacturers' instructions. For the quantification of gene expression, real time-PCR (RT-PCR) was performed on a Real Time System CFX96 (Bio-rad, Hercules, CA) or a LightCycler 480 (Roche, Basel, Switzerland) with a SYBR Premix Ex Taq II (Takara Bio Inc., Shiga, Japan) using the expression of β-actin as an internal control. For quantification, the second derivate maximum method was used for crossing point determination. Primer sets used in the present experiment are described in Online Resource 1.

Western Blot Analysis

Whole-cell lysate was prepared by a RIPA buffer (Sigma Aldrich) supplemented with proteinase and phosphatase inhibitors (Roche, Indianapolis, IN). Protein concentration was, then, determined by a bicinchoninic acid (BCA) method (Pierce BCA Protein Assay Kit, Thermo Scientific, Waltham, MA). After SDS-PAGE (sodium dodecyl sulfate–poly-acrylamide gel electrophoresis), separated proteins were blotted to a PDVF membrane (Hybond-P, GE healthcare, Buckinghamshire, UK) and blocked with an ECL plus blocking agent (GE healthcare). The membranes were then incubated with primary antibodies followed by incubation with an anti-IgG antibody conjugated by horseradish peroxidase (GE healthcare). Finally, the signal was detected by a chemiluminescent reagent (ECL Prime Western Blotting Detection System, GE healthcare). α-Tubulin was served as an internal control. Antibodies used in Western Blot analysis are described in Online Resource 1.

Statistical Analysis

Data are shown as box-and-whisker plots, and two groups were statistically compared using a Mann–Whitney U test. Statistical comparisons among more than two groups were conducted using a Kruskal–Wallis test followed by a Steel test. A p value smaller than 0.05 was defined as statistically significant.

Results

The Transient Outward Bulging of Arterial Walls at the Prospective Site of IA Formation

To elucidate machineries regulating the initiation of IAs, first, we examined sequential changes in histopathology of the lesion induced in a rat model during IA formation. In this model, IA formation is triggered by a left side of carotid ligation-induced increase of hemodynamic force at bifurcation sites of intracranial arteries, most typically at the contralateral (right) ACA-OA bifurcation [16]. As IA lesions with the two major histopathological features, a disrupted internal elastic lamina and degenerative changes of media, typically develop within 2 weeks after IA induction in our rat model, we prepared specimen from a right ACA-OA bifurcation every day until day 7 after the induction.

The size of IAs was progressively enlarged, once induced, during the experimental period at least until day 90 (Fig. 1a–c). Intriguingly, arterial walls at a right ACA-OA bifurcation, a prospective site of IA formation in our model, transiently bulged outwardly with the peak at day 2 and partially turned back in until day 5 after the induction (Fig. 1a–d). As the

internal elastic lamina was intact until day 4 (Fig. 1a, d) and the transient elevation of systemic blood pressure after IA induction was observed prior to the outward bulging of the arterial wall (Fig. 1d), this transient bulging at a right ACA-OA bifurcation was not the initiation of IA lesions but an event prior to the initiation presumably in response to elevation of systemic blood pressure and increase in a hemodynamic force due to a contralateral carotid ligation. In computational simulation of intracranial arteries, the maximal principal strain was observed certainly at the bifurcation site as observed in the histological sections from rats (Online Resource 5).

To corroborate presence of the outward bulging of arterial walls at bifurcation sites where IAs are induced, the real-time motion of the arterial wall at a right ACA-OA bifurcation was monitored in a live animal by an intra-vital multiphoton confocal microscopic examination. In this experiment, we used the transgenic rat line [17], in which open-reading frame of a florescent protein, GFP, was aligned downstream of tie-2 promoter/enhancer and endothelial cells are thus selectively visualized by endothelial cell-specific expression of GFP, to monitor wall motion of the bifurcation. Consistently with above findings in the histopathological analysis (Fig. 1), the arterial wall specifically at the right ACA-OA bifurcation site, the IA-prone site, was periodically and outwardly stretched (Fig. 2, Online Resource 6).

Involvement of Macrophages in the Outward Bulging of Intracranial Arterial Walls at the Prospective Site of IA Formation

As macrophages are major inflammatory cells in IA lesions [18, 19] and contribute to the maintenance of inflammation in situ to provide the microenvironment leading to the formation and the progression of the disease [5], we examined the number of infiltrating macrophages, CD68-positive cells in immunohistochemistry, at the earliest stage of IA formation. We found that the number of infiltrating macrophages in IA lesions was gradually increased until day 5 after IA induction. Noted that macrophages accumulated almost specifically at the adventitia of induced IA lesions (Fig. 3). Next, we examined effect of a pharmacological depletion of these infiltrating macrophages by clodronate liposome on the outward bulging of arterial walls of a prospective site of IA formation to clarify whether macrophages contribute to this outward bulging as well. Clodronate liposome treatment depleted about 81% of CD68-positive macrophages in spleen from the treated animal (Online Resource 2) and about a half of them in IA lesions (Fig. 4a, b). Such a depletion of macrophages in the lesion suppressed the outward bulging of arterial walls at the bifurcation site about 54% (Fig. 4c), suggesting the contribution of macrophage activity to this transient bulging
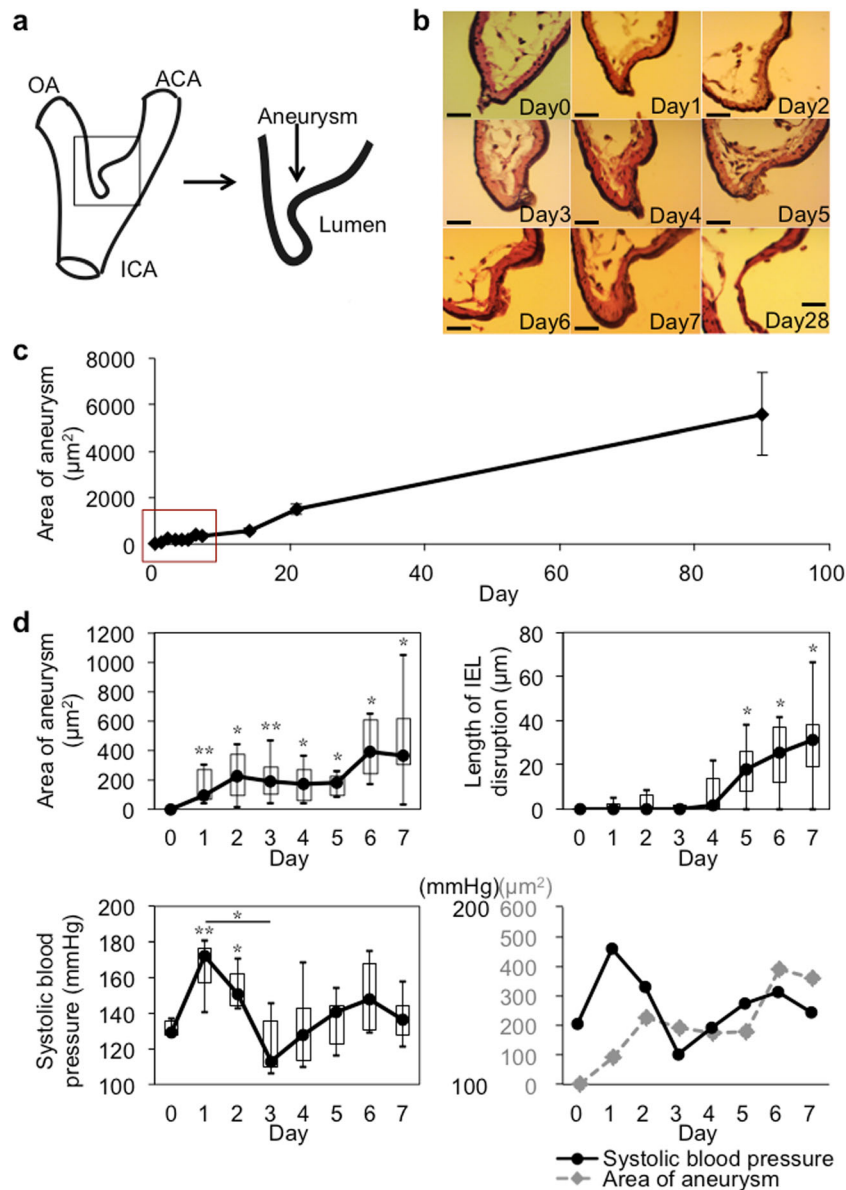
Fig. 1 Transient outward bulging of arterial walls at the earliest stage of IA formation in a rat model. **a** Schematic representation of IA lesions examined. ACA = anterior cerebral artery, OA = olfactory artery, ICA = internal carotid artery. **b** Sequential morphological changes of a prospective site of IA formation after the induction. The right ACA-OA bifurcation was harvested from rats subjected to IA induction before and from days 1 to 28 after the induction. Elastica van Gieson staining was done and representative images are shown. Bar = 20 μm. **c** Sequential changes in the size of induced IAs. The area of induced IAs at the right ACA-OA bifurcation was measured ($n = 5$, 9, 6, 8, 5, 7, 5, 10, 4, 8, and 7 in days 0, 1, 2, 3, 4, 5, 6, 7, 14, 21, and 90, respectively) and its sequential changes are shown in the graph. Data represents median ± SEM. **d** The

area, the distance of a disrupted internal elastic lamina (IEL) of induced IA lesions in rats (upper left and right panels) and systolic blood pressure of these rats (lower left panel). The right ACA-OA bifurcation was harvested from rats subjected to IA induction before and from days 1 to 7 after the induction. Systolic blood pressure of each rat was measured by a tail-cuff method. Elastica van Gieson staining was done and the area and the distance between the edges of a disrupted IEL of induced IAs were measured. Unified graph of upper and lower left panels is also shown in the lower right. Data represents box-and-whisker plots. Statistical analysis was done by a Kruskal–Wallis test followed by a Steel test. *$p < 0.05$, **$p < 0.01$

of arterial walls like the progression of IAs at the later stage [5]. Here, infiltrating macrophages mainly located at the adventitia secreted matrix metalloproteinase-9 (MMP-9), whose expression was remarkably suppressed in clodronate liposome-treated rats (Fig. 4d), and may contribute to reduce vascular stiffness and to facilitate the outward bulging.

## Trans-endothelial Cell Migration of Macrophages into IA Lesions

Based on the crucial role of macrophages in the pathogenesis of IAs, we next addressed a remaining but fundamental question of how this type of cells infiltrated in IA walls during its

Fig. 2 Real-time imaging of a prospective site of IA formation in a rat model. Serial freeze-frame images from a real-time imaging analysis of a prospective site of IA formation by a multiphoton-laser confocal microscopy system. The ACA-OA bifurcation site, a prospective site of IA formation, of a W-Tg(Tek-GFP)1Soh rat was surgically exposed and monitored. Serial freeze-frame images at about every 130 ms were obtained and traced out by a line. Serial freeze-frame images, magnified images corresponding to the white square and the overlaid images of each traced line at each time point are shown. Bar = 100 μm
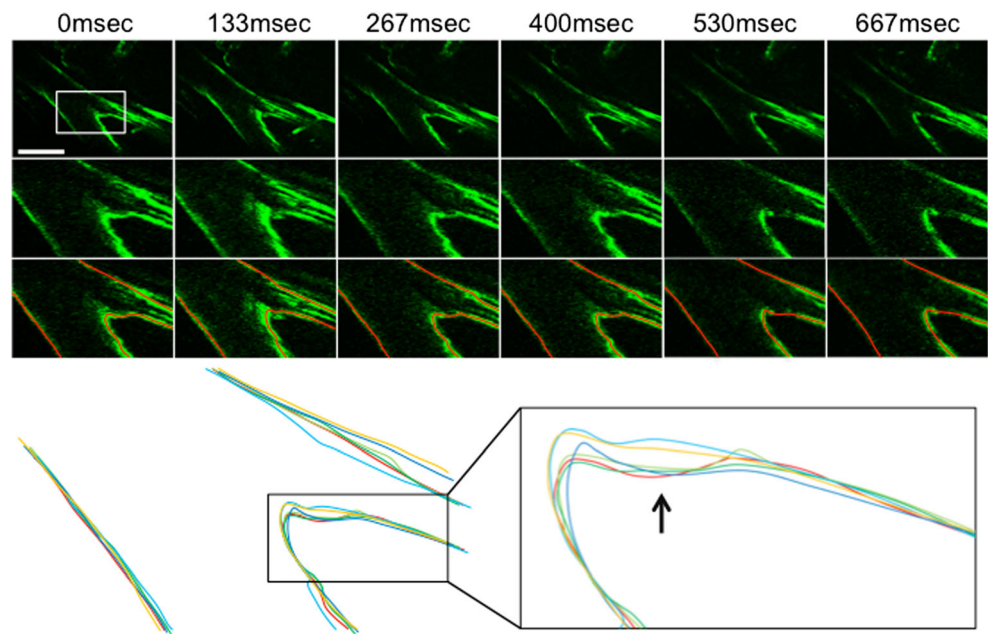

formation. We first histologically examined arterial walls of induced IA lesions in a rat model at day 5 by TEM, SEM, or SBF-SEM, and found some macrophages attached to the endothelial cells, some located in sub-endothelial space, or some at the adventitia of the lesion (Fig. 5a), suggesting the trans-endothelial migration of macrophages in lesions. To migrate into arterial walls across endothelial cells, structural barrier-like junctions between endothelial cells and an internal elastic lamina should be destructed. Consistently, disruption of an internal elastic lamina at lesions is the well-recognized

character of IAs. Observation by the electron microscopy revealed the moth-eaten appearance in the internal elastic lamina located at IA lesions at the earliest stage of IA formation (day 1) (Fig. 5b), suggesting that activated endothelial cells closely located degenerated this structure to facilitate macrophage infiltration. As to junctions between endothelial cells, some endothelial cells at the lesion were detached and continuity of endothelial cell layer was disturbed specifically at the site of IA formation (Fig. 5c). We then examined vascular permeability of IA walls to verify that discontinuity of endothelial cell
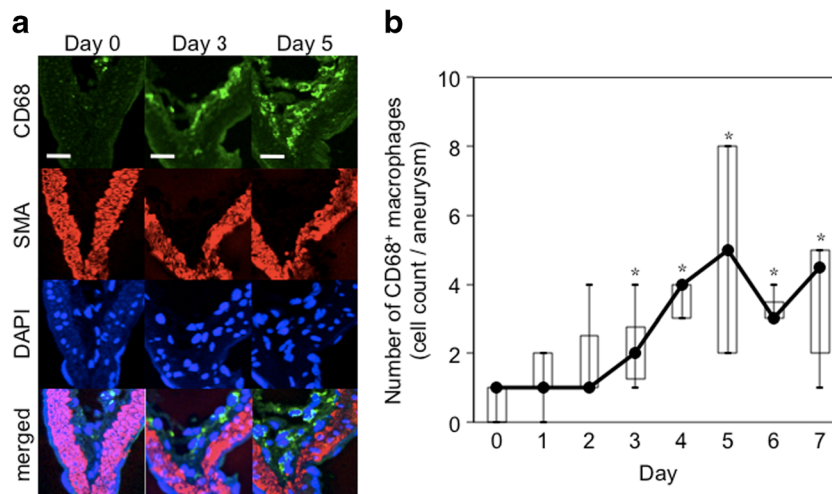
Fig. 3 Time course of macrophage infiltration in IA lesions induced in rats. IA lesions from rats subjected to IA induction (see "Methods" in detail) was harvested every day until day 7 ($n = 5, 9, 6, 8, 5, 7, 5$, and 8 in days 0, 1, 2, 3, 4, 5, 6, and 7, respectively) and immunostained. **a** Representative images of immunohistochemistry for CD68 (green), a

macrophage marker, for α-smooth muscle actin (SMA, red), a vascular smooth muscle marker, nuclear staining by DAPI (blue) and merged images are shown. Bar = 10 μm. **b** the number of CD68-positive cells is shown. Data represents box-and-whisker plots. Statistical analysis was done by a Kruskal–Wallis test followed by the Steel test. *$p < 0.05$
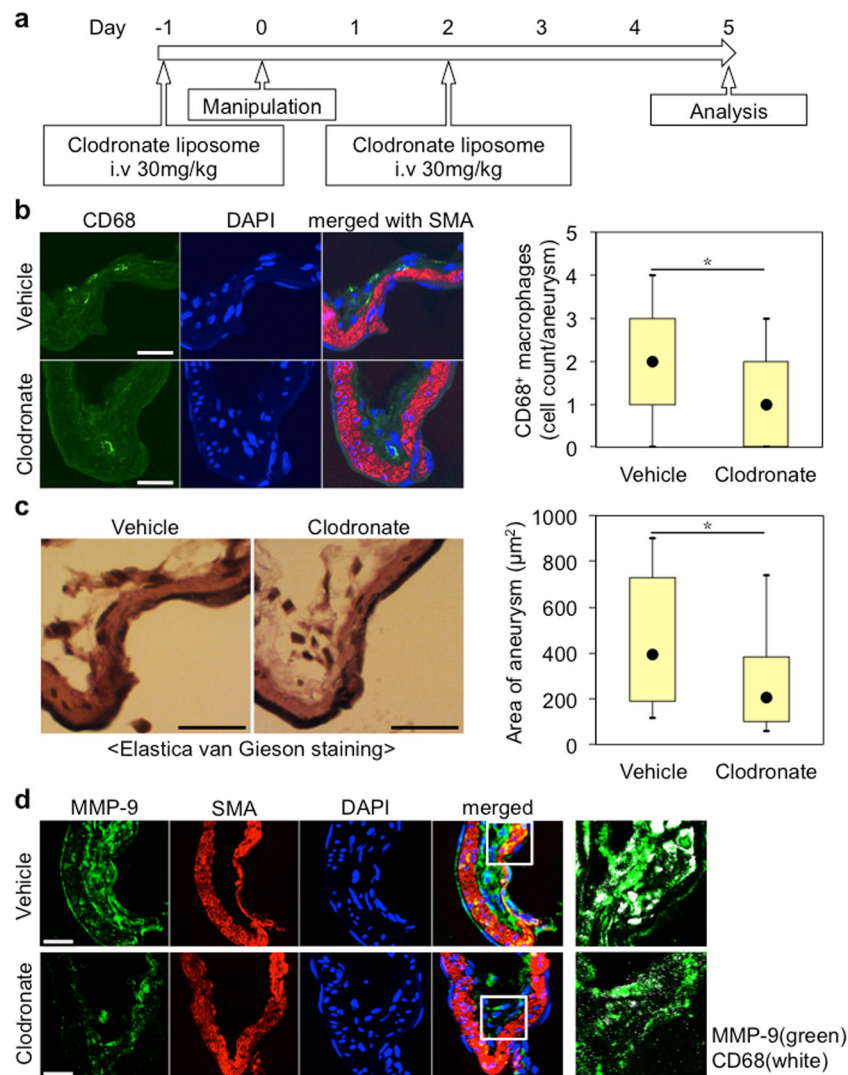
Fig. 4 Effect of macrophage function on the outward bulging of arterial walls at a prospective site of IA formation in a rat model. **a** Time course of the experiment. **b** Depletion of macrophages infiltrating in IA walls of rats treated with clodronate liposome. IA lesions at the right ACA-OA bifurcation were harvested from rats treated with clodronate liposome (30 mg/kg, clodronate, $n = 11$) or vehicle (vehicle, $n = 15$) and immunostained. Representative images of immunohistochemistry for CD68 (green), a macrophage marker, nuclear staining by DAPI (blue) and merged images with immunostained image for a vascular smooth muscle marker, α-smooth muscle actin (SMA, red), are shown in the left panels. Bar = 20 μm. In the right panel, cell count of CD68-positive cells, macrophages, is shown. Data represents box-and-whisker plots. Statistical analysis was done by a Mann–Whitney U test. $*p < 0.05$. **c** Effect of macrophage depletion on the size of induced IAs. IA lesions at the right

ACA-OA bifurcation were harvested and the size of induced IAs was measured (vehicle, $n = 18$, clodronate, $n = 12$). Representative images of Elastica van Gieson staining (EvG staining) of IA lesions are shown in the left panels and the size of these IAs is shown in the right panel. Bar = 20 μm. Data represents box-and-whisker plots. Statistical analysis was done by a Mann–Whitney U test. $*p < 0.05$. **d** Expression of matrix metalloproteinase-9 (MMP-9) in IA lesions and effect of clodronate liposome on its expression. IA lesions at the right ACA-OA bifurcation were harvested and immunostained. Representative images of immunohistochemistry for MMP-9 (green), SMA (red), nuclear staining by DAPI (blue), and merged images are shown in the left panels. In the right panels, representative magnified images of immunostaining corresponding to the white square in the left panels for MMP-9 (green) and CD68 (white) are shown. Bar = 20 μm

layer disturb barrier function of endothelial cells. Evans blue was intra-arterially injected in a rat model and leakage of this dye at the right ACA-OA bifurcation site was quantified using a choroid plexus, known as a tissue with sinusoid pattern of capillaries characterized by fenestrated basement membrane and the presence of an intercellular gap [20], as a positive control. In the choroid plexus only from Evans-blue-injected rats, Evans blue could be detected in extra-vascular space as

expected (Online Resource 3). In arterial walls at the ACA-OA bifurcation from Evans-blue-injected rats after IA induction, leakage of Evans blue in arterial walls was detected and its extent was significantly increased even as early as 6 h after IA induction compared with that from rats subjected to sham operation (Fig. 5d), supporting our assumption that macrophages infiltrate into arterial walls across destructed endothelial cell barrier at the prospective site of IA formation.
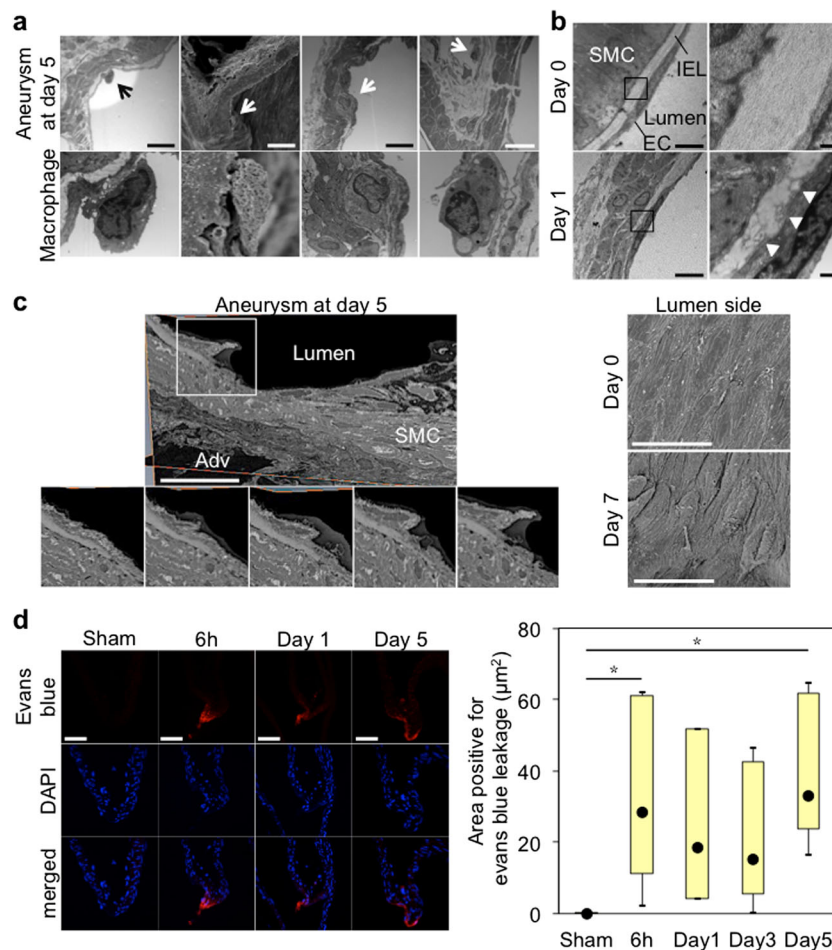
Fig. 5 Trans-endothelial cell migration of macrophages into IA lesions. **a** Location of macrophages in IA lesions. IA lesion at the right ACA-OA bifurcation of rats 5 days after IA induction was harvested and subjected to the electron microscopic examination. Representative images to show macrophages attached to endothelial cells, located at the sub-endothelial layer and at the adventitia are shown (arrow). Bar = 20 μm. **b** The moth-eaten destruction of the internal elastic lamina at the right ACA-OA bifurcation of rats before (day 0) and 1 day (day 1) after IA induction. Representative images of TEM and magnified images corresponding to the black square in the right panels are shown. White triangles indicate the moth-eaten destruction. Bar = 5 μm (left panels) and 500 nm (right panels). EC = endothelial cell, SMC = smooth muscle cell, IEL = internal elastic lamina. **c** Destructive changes in endothelial cell layer. IA lesion at the right ACA-OA bifurcation of rats before (day 0), 5 (day 5), or 7 (day 7) days after IA induction was harvested and subjected to SBF-SEM or SEM. Representative images of SBF-SEM (the left panel) and images of serial sections corresponding to the white square in the upper panel are shown in the left lower panels. Bar = 10 μm. Representative images of SEM are also shown in the right panels. Bar = 20 μm. **d** Disruption of the endothelial cell barrier at the site of IA formation in rats. Rats subjected to IA induction were maintained for 6 h, 1 (day 1), 3 (day 3), or 5 days (day 5) after the induction and injected Evans blue dye (45 mg/kg). Immediately after Evans blue injection, IA lesions at the right ACA-OA bifurcation were harvested and subjected to the observation by a fluorescent confocal microscope. Representative images of a fluorescent image of Evans blue, nuclear staining by DAPI and merged images are shown in the left panels. Bar = 50 μm. In the right panel, quantification of the area positive for Evans blue leakage is shown (n = 7, 5, 3, 5, 5 in sham, 6 h, days 1, 3, and 5, respectively). Data represents box-and-whisker plots. Statistical analysis was done by a Kruskal–Wallis test followed by the Steel test. *$p < 0.05$

Recruitment of Macrophages at the Adventitia of IA Lesions through CCL2 Produced from Activated Fibroblast by a Mechanical Stretch

Macrophages accumulate almost exclusively in the adventitia of lesions (Fig. 3) and regulate inflammatory responses there to induce and progress of the disease [5]. We, thus, tried to find out how machineries accumulate macrophages at the adventitia of the lesion. Through the electron microscopic examination, we identified fibroblasts as a most abundant type of cells in the adventitia (Fig. 6a) and also found the dramatic change of intracellular component of this type of cells, i.e., dramatically increase of rough endoplasmic reticulum and Golgi apparatus, suggesting activation of fibroblasts [21] (Fig. 6b, 3D-reconstructed fibroblasts are shown in Online Resource 7 (day 0) and 8 (day 5)). From these observations, we hypothesized that activated fibroblasts by a mechanical stretch located at the adventitia recruited macrophages to evoke inflammatory responses leading to IA formation. To address such an assumption, we used a primary culture of

Fig. 6 Morphological changes of fibroblasts after IA formation located at the adventitia of IA walls of rats. IA lesion at the right ACA-OA bifurcation of rats before (day 0) or 5 (day 5) after the induction was harvested and subjected to TEM (**a**) or SBF-SEM (**b**). Representative images of TEM or SBF-SEM are shown. In images from the SBF-SEM analyses, magnified images and colored images are also shown. In the lowest panels, 3D-reconstructed images of fibroblasts in which nucleus, rough endoplasmic reticulum or Golgi apparatus are colored in purple, red, or yellow, respectively. SMC = medial smooth muscle cells, Adv = adventitia. Bar = 10 μm (**a**) and 5 μm (**b**)
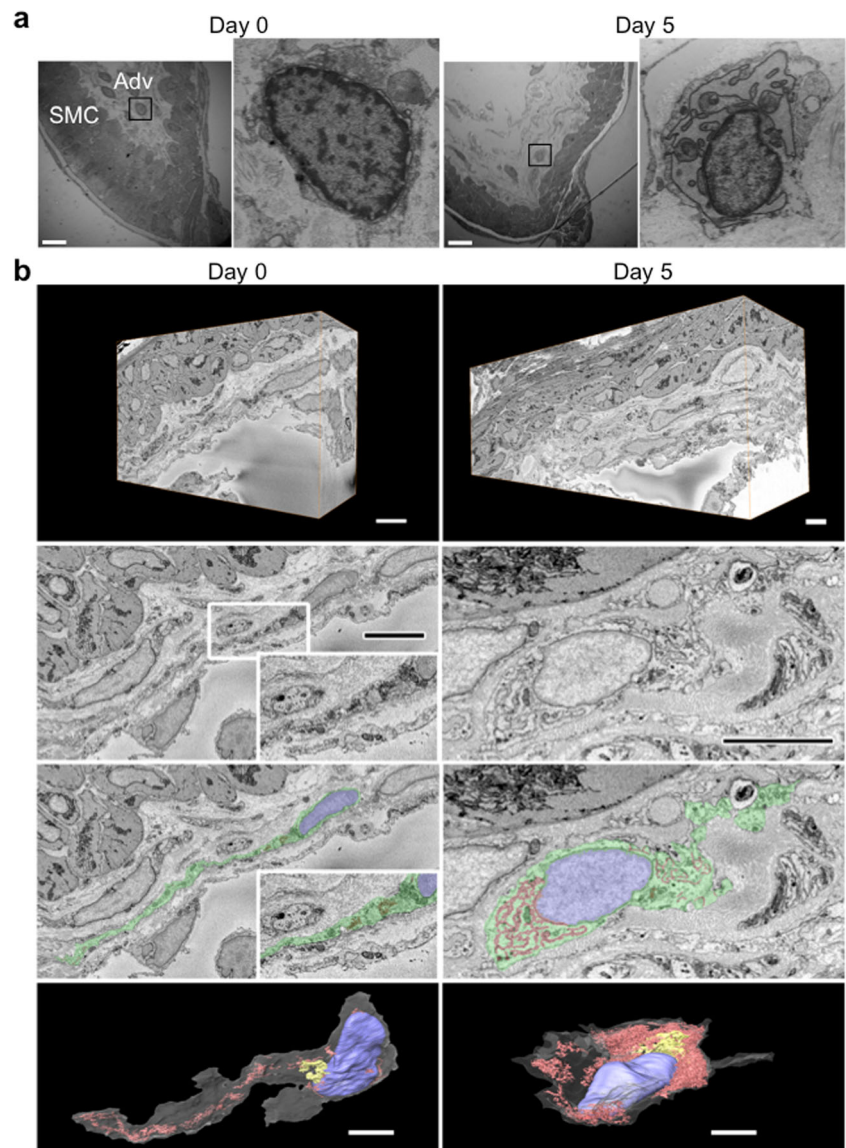
fibroblasts prepared from an adventitia of human aorta (Online Resource 4a) and subjected this primary culture to a mechanical stretch. Consistently with the previous report [22], phosphorylation of ERK was upregulated in this primary culture in response to a mechanical stretch loading at the strength- and time-dependent manner (Online Resource 4b). In an animal model, phosphorylation of ERK was detected in cells located exclusively at the adventitia, presumably fibroblasts, already at day 1 and signals for phosphorylated ERK was increased at day 5 after IA induction (Online Resource 4c), providing the in vivo relevance of above in vitro results (Online Resource 4b). We next examined whether fibroblasts recruited macrophages upon activation by a mechanical stretch loading. In a Transwell system, the conditioned medium from the fibroblast culture loaded by a mechanical stretch (10%, 1 Hz, 3 h) recruited significantly more THP-1 cells used

as alternatives of peripheral monocytes into a lower chamber (Fig. 7a). We then performed RT-PCR analysis to clarify whether a mechanical stretch could induce expression of chemoattractant factors for macrophages and if yes what. We found that expression of *CCL2* and *CCL7* was significantly upregulated in a mechanical stretch-loaded group (10%, 1 Hz, 3 h) (Fig. 7b) and a multiplex array analysis of cytokines supported the increase of CCL2 protein in the culture medium of fibroblasts subjected to a mechanical stretch (Fig. 7c and Online Resource 9), supporting our assumption that stretched fibroblasts could recruit macrophages to the adventitia of intracranial arteries to evoke inflammation there. Mechanical stretch-induced activated fibroblasts at the adventitia may more actively participate in inflammation at the site of IA formation than merely recruitment of macrophages, because activated fibroblasts secreted some cytokines like IL-1β, into
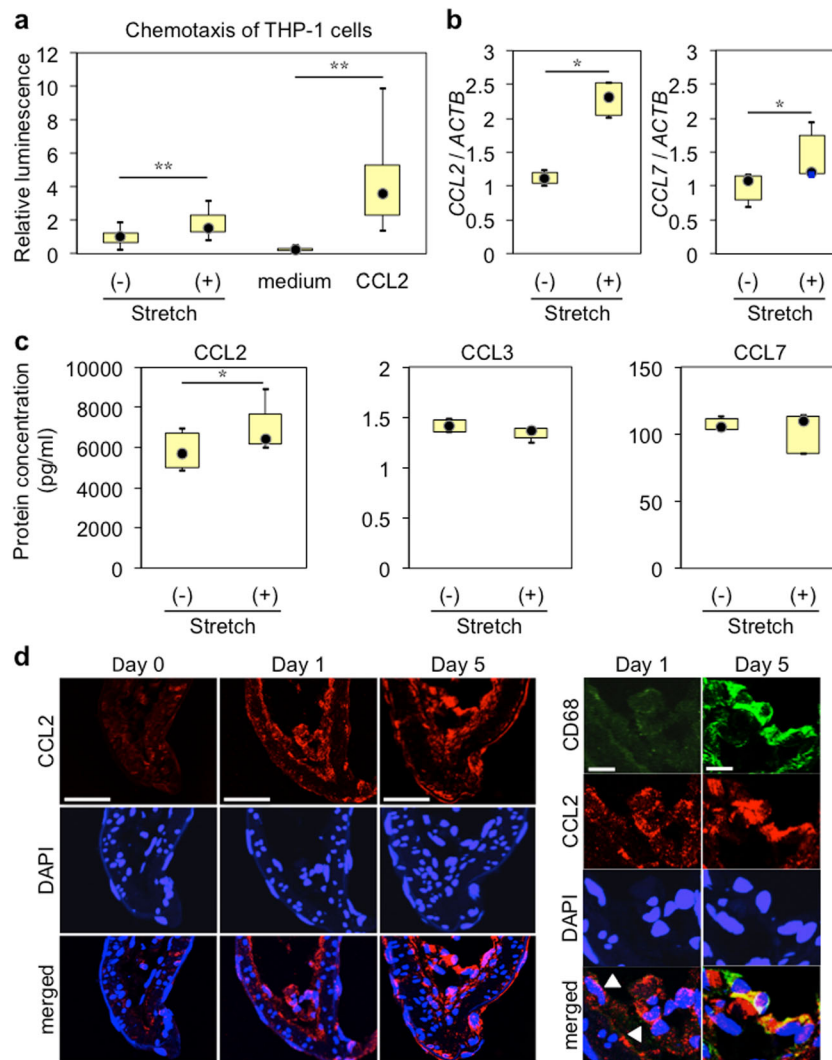
Fig. 7 Chemotaxis of THP-1 cells by mechanical stretch-loaded fibroblasts via CCL2. **a** Chemotactic activity to THP-1 cells of the supernatant from mechanical stretch-loaded fibroblasts. Primary culture of adventitial fibroblasts was loaded by a mechanical stretch (10%, 1 Hz, 3 h) and the supernatant was collected. Chemotactic activity of this supernatant to THP-1 cells was examined by a Transwell system using CCL2 (100 ng/mL) as a positive control. Luminescence reflecting number of cells migrated into a lower chamber was measured and relative luminescence was calculated (Stretch (−), Stretch (+), medium, CCL2, $n = 24, 24, 22, 22$, respectively). Data represents box-and-whisker plots. Statistical analysis was done by a Mann–Whitney U test. $**p < 0.01$. **b** Induction of *CCL2* and *CCL7* mRNA expression by a mechanical stretch in cultured fibroblasts. Primary culture of adventitial fibroblasts was loaded by a mechanical stretch (10%, 1 Hz, 3 h) and total RNA was prepared. mRNA expression of chemoattractants for macrophages was assessed by RT-PCR analysis (Stretch (−) and Stretch (+), $n = 4$ for each group). Data represents box-and-whisker plots. Statistical analysis was done by a Mann–Whitney

U test. $*p < 0.05$. **c** Induction of CCL2 protein expression by a mechanical stretch in cultured fibroblasts. Primary culture of adventitial fibroblasts was loaded by a mechanical stretch (10%, 1 Hz, 3 h) and the supernatant was collected followed by a quantification of cytokines by a Multiplex assay (Stretch (−) and Stretch (+), $n = 4$ and 7, respectively). Data represents box-and-whisker plots. Statistical analysis was done by a Mann–Whitney U test. $*p < 0.05$. **d** Expression of CCL2 in IA lesions of rats. IA lesion at the right ACA-OA bifurcation of rats before, 1 (day 1), or 5 (day 5) days after IA induction was harvested and subjected to immunohistochemistry for CCL2. Representative images of immunostaining for CCL2 (red), nuclear staining by DAPI (blue) and merged images are shown in the left panels. In the right panels, representative images of immunostaining for CD68 (green), CCL2 (red), nuclear staining by DAPI (blue) and merged images are shown. White triangles indicate cells positive for CCL2 staining other than macrophages, presumably fibroblasts. Bar = 20 μm (left panels) and 10 μm (right panels)

the supernatant (Online Resource 9). In immunohistochemistry of IA lesions at the earliest stage of IA formation (day 1), CCL2 expression was detected at the adventitia of the lesion and positive signals for CCL2 staining was negative for macrophage marker CD68 (Fig. 7d), suggesting expression of

CCL2 in fibroblasts and providing in vivo relevance. Intriguingly, at day 5 after IA induction, some cells positive for CCL2 staining was also positive for CD68 staining (Fig. 7d), suggesting the formation of auto-amplification loop among macrophages as we demonstrated previously [5].

Discussion

Accumulating evidence, obtained from CFD analyses of human IA lesions or the ring of Willis and also in animal models, has implicated a crucial role of high WSS loaded on endothelial cells of intracranial arterial walls at their bifurcations as a trigger of IA formation [9, 10]. These studies have consistently demonstrated the close correlation of high WSS loading with sites of the initiation of IAs [9, 10]. We furthermore previously demonstrated that high WSS could induce expression of prostaglandin E receptor subtype EP2 and an inducible form of prostaglandin-producing enzyme, cyclooxygenase-2 (COX-2), in primary culture of endothelial cells to evoke prostaglandin-mediated inflammation in these cells and may facilitate macrophage recruitment to the lesion presumably via inducing CCL2 by EP2-mediated NF-κB activation and EP2-dependent stabilization of mRNA [8, 23]. However, it is still unclear whether high WSS is solely important for the initiation of the disease. This question is important for understanding the underlying pathogenesis because IA usually develops singly [24] but by contrast high WSS is basically loaded on every bifurcation sites. To address these remaining but important issues, in the present study, we examined the earliest events in the process of IA formation using an animal model and revealed some important findings. Intracranial arterial wall at the bifurcation site was transiently dilated in concert with the elevation of systemic blood pressure at the earliest stage of IA formation (only within a few days) and histological changes including disruption of internal elastic lamina and infiltration of CD68$^+$ cells in lesions was followed. As the pharmacological depletion of macrophages by clodronate liposome inhibited the size of IAs at the early stage (day 5), macrophages function to initiate IAs in response to hemodynamic stress in the earliest stage as similar in the latter stage [4, 6]. However, there is a structural barrier, an internal elastic lamina, to interfere migration of macrophages into adventitia even if fibroblasts there produced CCL2 in response to a mechanical stretch. TEM images of IA walls at the earliest stage of formation suggested the invasion of this structure by adjusting endothelial cells (Fig. 5b) presumably activated due to high WSS by increased blood flow and systemic blood pressure. Therefore, the initiation of IAs may be triggered by two distinct mechanical forces, high WSS, and mechanical stretch, and these two forces activate various types of cells in arterial walls not only to recruit macrophages into the adventitia but also to disrupt an internal elastic lamina to facilitate trans-endothelial migration of macrophages.

It is no doubt that the prevention of rupture of IAs is a most critical issue about IAs for our society. Currently, some part of unruptured IAs are selected as rupture-prone ones by some clinical or morphological features such as an age, a size, and a shape of each lesion, a past history of subarachnoid hemorrhage or by a confounding disease which increases the risk of surgical manipulation, and surgically treated with informed consent [25]. But many IAs, more than half in Japan [25], which have a low estimated risk of rupture or a high surgical risk, are followed without treatment except for ones targeting risk factors promoting rupture-like hypertension because of the lack of medical therapy complementary for surgical manipulations. As a natural consequence, sometimes IAs under follow-up rupture resulting in a devastating outcome. On the contrary, IAs not prone-to rupture are sometimes surgically manipulated with a risk of complication. To overcome such a current situation and properly identify rupture-prone IAs among much more stable ones, a novel method to qualitatively diagnose each lesion is essential. In addition, recurrence of IAs once after IAs are surgically and successfully treated at the time is another problem to be addressed. In the present study, we found the crucial role of fibroblasts activated by a mechanical stretch and subsequent macrophage infiltration in the initiation of IAs. In these points of view, activation of fibroblasts in the adventitia and macrophages could be a target for detecting recurrent and developing IAs. Recently, the potential of macrophage imaging as a diagnostic method to detect rupture-prone lesions have been demonstrated [26]. In these series of studies, iron-containing nanoparticles are intravenously injected and macrophages engulfing these particles are visualized by MRI T2* sequence [26]. Authors further histologically demonstrated that lesions positive for this imaging technique certainly contains macrophages engulfing iron-containing nanoparticles [27]. Intriguingly, the treatment with non-steroidal anti-inflammatory drugs (NSAIDs) reduces signals in macrophage imaging by MRI [28], suggesting the potential of this imaging technique as a diagnostic method to examine inflammatory status in each IA lesion examined. Given the previous case-control study that the frequent usage of NSAIDs reduces the risk of subarachnoid hemorrhage [29], macrophage imaging may be an ideal method to identify rupture-prone IAs among many stable ones. However, based on recent strengthened warning from the Food and Drug Administration (FDA) regarding the usage of ferumoxytol, FDA approved an iron-containing nanoparticle to this imaging technique because of the risk of serious allergic reactions (https://www.fda.gov/Drugs/DrugSafety/ucm440138.htm) and also on the technical difficulty in subtraction of images obtained from MRI analysis [27], a novel imaging reagent to monitor the presence of macrophages in lesions or activation of fibroblasts which recruits these cells is waited to be developed.

Compliance with Ethical Standards

Conflict of Interest T. A. was supported by the Coordination Fund from the Japanese Ministry for Education, Culture, Sports, Science and Technology (MEXT) and Astellas Pharma Inc. to Kyoto University until 31th/March/2017 and S.N. is supported by a same grant. S.N. is a scientific advisor to Astellas Pharma. H. K., H. M., S. S., N.O., K. M., K. S., K. Y., K. N., and H. K. declare that they have no conflict of interest.

Ethical Approval All applicable international, national, and/or institutional guidelines for the care and use of animals were followed. And this study was approved by the Institutional Animal Care and Use Committee of Kyoto University Graduate School of Medicine and also of National Cerebral and Cardiovascular Center. All procedures performed in studies involving human participants were in accordance with the ethical standards of the institutional and/or national research committee and with the 1964 Helsinki declaration and its later amendments or comparable ethical standards. This study was approved by the Institutional Review Board of Shimizu Hospital (Kyoto, Japan, Approval No. 203). Informed consent was obtained from all individual participants included in the study.

Publisher's Note Springer Nature remains neutral with regard to jurisdictional claims in published maps and institutional affiliations.

References

1. Juvela S, Poussa K, Porras M. Factors affecting formation and growth of intracranial aneurysms: a long-term follow-up study. Stroke. 2001;32(2):485–91.
2. van Gijn J, Kerr RS, Rinkel GJ. Subarachnoid haemorrhage. Lancet. 2007;369(9558):306–18. https://doi.org/10.1016/S0140-6736(07)60153-6.
3. Aoki T, Kataoka H, Shimamura M, Nakagami H, Wakayama K, Moriwaki T, et al. NF-kappaB is a key mediator of cerebral aneurysm formation. Circulation. 2007;116(24):2830–40. https://doi.org/10.1161/CIRCULATIONAHA.107.728303.
4. Aoki T, Kataoka H, Ishibashi R, Nozaki K, Egashira K, Hashimoto N. Impact of monocyte chemoattractant protein-1 deficiency on cerebral aneurysm formation. Stroke. 2009;40(3):942–51. https://doi.org/10.1161/STROKEAHA.108.532556.
5. Aoki T, Frosen J, Fukuda M, Bando K, Shioi G, Tsuji K, et al. Prostaglandin E2-EP2-NF-kappaB signaling in macrophages as a potential therapeutic target for intracranial aneurysms. Sci Signal. 2017;10(465). https://doi.org/10.1126/scisignal.aah6037.
6. Kanematsu Y, Kanematsu M, Kurihara C, Tada Y, Tsou TL, van Rooijen N, et al. Critical roles of macrophages in the formation of intracranial aneurysm. Stroke. 2011;42(1):173–8. https://doi.org/10.1161/STROKEAHA.110.590976.
7. Aoki T, Kataoka H, Nishimura M, Ishibashi R, Morishita R, Miyamoto S. Regression of intracranial aneurysms by simultaneous inhibition of nuclear factor-kappaB and Ets with chimeric decoy oligodeoxynucleotide treatment. Neurosurgery. 2012;70(6):1534–43; discussion 43. https://doi.org/10.1227/NEU.0b013e318246a390.
8. Aoki T, Nishimura M, Matsuoka T, Yamamoto K, Furuyashiki T, Kataoka H, et al. PGE(2)-EP(2) signalling in endothelium is activated by haemodynamic stress and induces cerebral aneurysm through an amplifying loop via NF-kappaB. Br J Pharmacol. 2011;163(6):1237–49. https://doi.org/10.1111/j.1476-5381.2011.01358.x.
9. Meng H, Wang Z, Hoi Y, Gao L, Metaxa E, Swartz DD, et al. Complex hemodynamics at the apex of an arterial bifurcation induces vascular remodeling resembling cerebral aneurysm initiation. Stroke. 2007;38(6):1924–31. https://doi.org/10.1161/STROKEAHA.106.481234.
10. Kulcsar Z, Ugron A, Marosfoi M, Berentei Z, Paal G, Szikora I. Hemodynamics of cerebral aneurysm initiation: the role of wall shear stress and spatial wall shear stress gradient. AJNR Am J Neuroradiol. 2011;32(3):587–94. https://doi.org/10.3174/ajnr.A2339.
11. Cebral J, Ollikainen E, Chung BJ, Mut F, Sippola V, Jahromi BR, et al. Flow conditions in the intracranial aneurysm lumen are associated with inflammation and degenerative changes of the aneurysm wall. AJNR Am J Neuroradiol. 2017;38(1):119–26. https://doi.org/10.3174/ajnr.A4951.
12. Shojima M, Oshima M, Takagi K, Torii R, Hayakawa M, Katada K, et al. Magnitude and role of wall shear stress on cerebral aneurysm: computational fluid dynamic study of 20 middle cerebral artery aneurysms. Stroke. 2004;35(11):2500–5. https://doi.org/10.1161/01.STR.0000144648.89172.0f.
13. Yamamoto R, Aoki T, Koseki H, Fukuda M, Hirose J, Tsuji K, et al. A sphingosine-1-phosphate receptor type 1 agonist, ASP4058, suppresses intracranial aneurysm through promoting endothelial integrity and blocking macrophage transmigration. Br J Pharmacol. 2017;174(13):2085–101. https://doi.org/10.1111/bph.13820.
14. Huang P, Zhou CM, Qin H, Liu YY, Hu BH, Chang X, et al. Cerebralcare granule (R) attenuates blood-brain barrier disruption after middle cerebral artery occlusion in rats. Exp Neurol. 2012;237(2):453–63. https://doi.org/10.1016/j.expneurol.2012.07.017.
15. Hed J, Dahlgren C, Rundquist I. A simple fluorescence technique to stain the plasma membrane of human neutrophils. Histochemistry. 1983;79(1):105–10.
16. Aoki T, Nishimura M. Targeting chronic inflammation in cerebral aneurysms: focusing on NF-kappaB as a putative target of medical therapy. Expert Opin Ther Targets. 2010;14(3):265–73. https://doi.org/10.1517/14728221003586836.
17. Ohtsuki S, Kamiya N, Hori S, Terasaki T. Vascular endothelium-selective gene induction by Tie2 promoter/enhancer in the brain and retina of a transgenic rat. Pharm Res. 2005;22(6):852–7. https://doi.org/10.1007/s11095-005-4579-y.
18. Frosen J, Piippo A, Paetau A, Kangasniemi M, Niemela M, Hernesniemi J, et al. Remodeling of saccular cerebral artery aneurysm wall is associated with rupture: histological analysis of 24 unruptured and 42 ruptured cases. Stroke. 2004;35(10):2287–93. https://doi.org/10.1161/01.STR.0000140636.30204.da.
19. Aoki T, Kataoka H, Morimoto M, Nozaki K, Hashimoto N. Macrophage-derived matrix metalloproteinase-2 and -9 promote the progression of cerebral aneurysms in rats. Stroke. 2007;38(1):162–9. https://doi.org/10.1161/01.STR.0000252129.18605.c8.
20. Johanson CE, Stopa EG, McMillan PN. The blood-cerebrospinal fluid barrier: structure and functional significance. Methods Mol Biol. 2011;686:101–31. https://doi.org/10.1007/978-1-60761-938-3_4.
21. Ghadially FN. Ultrastructural pathology of the cell and matrix: third edition volume I. Boston: Butterworth-Heinemann; 2013.
22. Wang JG, Miyazu M, Matsushita E, Sokabe M, Naruse K. Uniaxial cyclic stretch induces focal adhesion kinase (FAK) tyrosine phosphorylation followed by mitogen-activated protein kinase (MAPK) activation. Biochem Biophys Res Commun. 2001;288(2):356–61. https://doi.org/10.1006/bbrc.2001.5775.
23. Aoki T, Narumiya S. Prostaglandins and chronic inflammation. Trends Pharmacol Sci. 2012;33(6):304–11. https://doi.org/10.1016/j.tips.2012.02.004.

24. Hishikawa T, Date I, Tokunaga K, Tominari S, Nozaki K, Shiokawa Y, et al. Risk of rupture of unruptured cerebral aneurysms in elderly patients. Neurology. 2015;85(21):1879–85. https://doi.org/10.1212/WNL.0000000000002149.

25. Morita A, Kirino T, Hashi K, Aoki N, Fukuhara S, Hashimoto N, et al. The natural course of unruptured cerebral aneurysms in a Japanese cohort. N Engl J Med. 2012;366(26):2474–82. https://doi.org/10.1056/NEJMoa1113260.

26. Hasan D, Chalouhi N, Jabbour P, Dumont AS, Kung DK, Magnotta VA, et al. Early change in ferumoxytol-enhanced magnetic resonance imaging signal suggests unstable human cerebral aneurysm: a pilot study. Stroke. 2012;43(12):3258–65. https://doi.org/10.1161/STROKEAHA.112.673400.

27. Aoki T, Saito M, Koseki H, Tsuji K, Tsuji A, Murata K, et al. Macrophage imaging of cerebral aneurysms with ferumoxytol: an exploratory study in an animal model and in patients. J Stroke Cerebrovasc Dis. 2017;26(10):2055–64. https://doi.org/10.1016/j.jstrokecerebrovasdis.2016.10.026.

28. Hasan DM, Chalouhi N, Jabbour P, Dumont AS, Kung DK, Magnotta VA, et al. Evidence that acetylsalicylic acid attenuates inflammation in the walls of human cerebral aneurysms: preliminary results. J Am Heart Assoc. 2013;2(1):e000019. https://doi.org/10.1161/JAHA.112.000019.

29. Hasan DM, Mahaney KB, Brown RD Jr, Meissner I, Piepgras DG, Huston J, et al. Aspirin as a promising agent for decreasing incidence of cerebral aneurysm rupture. Stroke. 2011;42(11):3156–62. https://doi.org/10.1161/STROKEAHA.111.619411.